Testing a 95 GeV Scalar at the CEPC with Machine Learning*

Yabo Dong (董亚博)[1] Manqi Ruan (阮曼奇)[2] Kun Wang (王坤)[3†] Haijun Yang (杨海军)[4] Jingya Zhu (朱经亚)[1‡]

[1]School of Physics and Electronics, Henan University, Kaifeng 475004, China
[2]Institute of High Energy Physics, Chinese Academy of Sciences, Beijing 100049, China
[3]College of Science, University of Shanghai for Science and Technology, Shanghai 200093, China
[4]State Key Laboratory of Dark Matter Physics, Key Laboratory for Particle Astrophysics and Cosmology (MOE), Shanghai Key Laboratory for Particle Physics and Cosmology (SKLPPC), School of Physics and Astronomy & Tsung-Dao Lee Institute, Shanghai Jiao Tong University, Shanghai 200240, China

Abstract: Several possible excesses around 95 GeV hint at an additional light scalar beyond the Standard Model. We examine the capability of the Circular Electron-Positron Collider (CEPC) to test this hypothesis in the Higgs-strahlung channel $e^+e^- \to ZS$ with $Z \to \mu^+\mu^-$ and $S \to \tau^+\tau^-$. A full detector simulation shows that the optimal center-of-mass energy for studying the 95 GeV light scalar is 210 GeV. A deep neural network classifier reduces the luminosity required for discovery by half. At $L = 20\ \text{ab}^{-1}$, the 5σ sensitivity of the CEPC to the signal strength $\mu_{\tau\tau}^{ZS}$ reaches 0.016 and 0.020 for $\sqrt{s} = 210$ GeV and 240 GeV, respectively. The corresponding thresholds for a 5% precision measurement are $\mu_{\tau\tau}^{ZS} > 0.10$ and > 0.12. At $\sqrt{s} = 210$ GeV (240 GeV), the 5σ coverage of all N2HDM-Flipped samples with $\chi^2_{h_{95}} < 7.82$ requires $L = 800\ \text{fb}^{-1}$ ($1.22\ \text{ab}^{-1}$). These results establish a 210 GeV run, augmented by machine-learning selection, as the most efficient strategy to confirm or refute the 95 GeV excess at future lepton colliders.

Keywords: new physics, collider phenomenology, CEPC, non-SM Higgs bosons, machine learning

DOI: 10.1088/1674-1137/ae2ebc **CSTR:** CSTR: 32044.14.ChinesePhysicsC.50031001

I. INTRODUCTION

Following the discovery of the 125 GeV Standard Model (SM)-like Higgs boson at the Large Hadron Collider (LHC) [1, 2], the possibility of additional scalar particles has attracted considerable attention. Although the SM contains only one fundamental scalar, there is no symmetry preventing the existence of more. Such additional scalars are theoretically motivated as they may play essential roles in addressing baryon asymmetry, electroweak phase transition, and dark matter [3−5].

Intriguingly, multiple experiments have reported possible local excesses near 95 GeV in different channels, including $b\bar{b}$ at LEP [6], $\gamma\gamma$ at CMS and ATLAS [7, 8], and $\tau^+\tau^-$ at CMS [9]. These excesses can be characterized by the following signal strength modifiers [10]:

$$\begin{aligned}
\mu_{bb}^{\text{exp}} &= \frac{\sigma_{\text{BSM}}(e^+e^- \to ZS(\to b\bar{b}))}{\sigma_{\text{SM}}(e^+e^- \to Zh_{95}(\to b\bar{b}))} = 0.117 \pm 0.057, \\
\mu_{\tau\tau}^{\text{exp}} &= \frac{\sigma_{\text{BSM}}(gg \to S \to \tau^+\tau^-)}{\sigma_{\text{SM}}(gg \to h_{95} \to \tau^+\tau^-)} = 1.2 \pm 0.5, \\
\mu_{\gamma\gamma}^{\text{exp}} &= \frac{\sigma_{\text{BSM}}(gg \to S \to \gamma\gamma)}{\sigma_{\text{SM}}(gg \to h_{95} \to \gamma\gamma)} = 0.24^{+0.09}_{-0.08}, \qquad (1)
\end{aligned}$$

where S denotes a hypothetical new scalar, and h_{95} is the SM Higgs boson with the mass rescaled to 95 GeV. It is worth noting that another CMS report on the $S \to \tau\tau$ channel in association with top quark pairs [11] presents results that differ from the di-tau excess discussed here. As that analysis remains preliminary, without subsequent updates, we focus our discussion on the currently available and more finalized results [9].

Received 18 August 2025; Accepted 16 December 2025; Accepted manuscript online 17 December 2025

* This work was supported by the National Natural Science Foundation of China under Grant No. 12275066 and by the startup research funds of Henan University. The work of K. Wang was also supported by the Open Project of the Shanghai Key Laboratory of Particle Physics and Cosmology under Grant No. 22DZ2229013-3. The work of M. Ruan was also supported by the National Key Program for S&T Research and Development under Contract No. 2024YFA1610603. The work of H. Yang was also supported by the National Natural Science Foundation of China under Grant No. W2441004.

† E-mail: kwang@usst.edu.cn
‡ E-mail: zhujy@henu.edu.cn

These hints have stimulated a broad range of phenomenological studies on simple extensions of the SM [12–23], multi-Higgs model [10, 24–49], supersymmetric models [50–63], and Georgi-Machacek models [64–68]. Ref. [69] presents the light Higgs (lighter than 120 GeV) discovery potential at the International Linear Collider (ILC) in the $S \to b\bar{b}$ decay channel and a center-of-mass energy of $\sqrt{s} = 250$ GeV. Ref. [70] provides the exclusion limit on the Z-light Higgs coupling at the ILC in the Higgs-strahlung process with decay channel independence. Through the study of the $S \to \tau\tau$ decay channel, Ref. [71] states that, in the search for a light Higgs, the search sensitivity for the $S \to \tau\tau$ decay channel is higher than that for the decay channel-independent one. Ref. [39] features the potential of the Circular Electron-Positron Collider (CEPC) to probe this hypothetical scalar through the $S \to b\bar{b}$ channel, considering a center-of-mass energy of $\sqrt{s} = 250$ GeV.

Among the observed anomalies, the possible excess in the $\tau^+\tau^-$ channel is even more pronounced, and in certain beyond the SM (BSM) scenarios, such as the two Higgs doublet model (2HDM) [72], the decay of $S \to \tau^+\tau^-$ can be enhanced significantly. This motivates a dedicated investigation into the $\tau^+\tau^-$ final state. The CEPC, primarily designed for precision measurements of the 125 GeV SM-like Higgs boson, is expected to operate at $\sqrt{s} = 240$ GeV with an integrated luminosity of approximately 20 ab^{-1} [73–76]. However, as a 95 GeV scalar is significantly lighter than the design target of the CEPC, the optimal center-of-mass energy ($\sqrt{s}$) for its discovery remains to be systematically assessed. Motivated by these considerations, the first part of this study is dedicated to identifying the optimal collision energy for probing a light Higgs with a mass near 95 GeV. In addition, we investigate the discovery potential of a light Higgs boson at 95 GeV in the $S \to \tau\tau$ decay channel by employing machine learning (ML) techniques such as eXtreme Gradient Boosting (XGBoost), Gradient Boosting Decision Tree (GBDT), and deep neural networks (DNNs) to enhance the sensitivity. Furthermore, a detailed analysis is performed to evaluate the expected precision of the $Z-S$ coupling and the branching ratio of $S \to \tau\tau$ at the CEPC. Finally, as a concrete example, we apply our approach within the Next-to 2HDM (N2HDM) to assess its capability in testing specific new physics scenarios.

II. MONTE CARLO SIMULATION

We investigate the process $e^+e^- \to Z(\to \mu^+\mu^-)S(\to \tau^+\tau^-)$ at the CEPC. The dominant irreducible background is $e^+e^- \to Z(\to \mu^+\mu^-)\tau^+\tau^-$, hereafter denoted as $Z\tau\tau$, which contains the same final - state topology as the signal. A sizable reducible background arises from $e^+e^- \to Z(\to \mu^+\mu^-)XX$ $(X = j, e, \mu)$, collectively labeled Zjj, where one or two X objects can be mis-tagged as hadronic τ jets. Signal and background events are simulated using MadGraph5_aMC@NLO_v3.4.2 [77, 78], interfaced to PYTHIA 8.2 [79] for parton showering and hadronization and Delphes 3.5.0 [80] for detector simulation using the CEPC baseline card, with τ-jets identified at an efficiency of 80% [81].

Owing to the difficulty of reconstructing τ decays, we employ the recoil mass observable [82], which allows the invariant mass of the scalar S to be inferred without relying on the reconstruction of its decay products. The recoil mass is defined as

$$M_{\text{recoil}} \equiv \sqrt{s + M^2_{\mu^+\mu^-} - 2\sqrt{s}(E_{\mu^+} + E_{\mu^-})}, \tag{2}$$

and it depends only on the well-measured four-momentum of the muon pair. This observable is robust against τ-decay ambiguities and provides strong discriminating power between the signal and background.

Figure 1 shows the M_{recoil} distributions for the signal ZS with $M_S = 95.5$ GeV, backgrounds $Z\tau\tau$ and Zjj, total (signal + background), and ratio of the total to the background. The number of signal events is normalized to 0.2, reflecting the assumption that the signal cross section is 20% of the SM prediction, whereas the background event numbers are normalized to 1. The signal exhibits a pronounced peak around M_S, whereas both backgrounds show broader distributions peaking near 91 GeV, consistent with the Z mass. The total distribution is background-

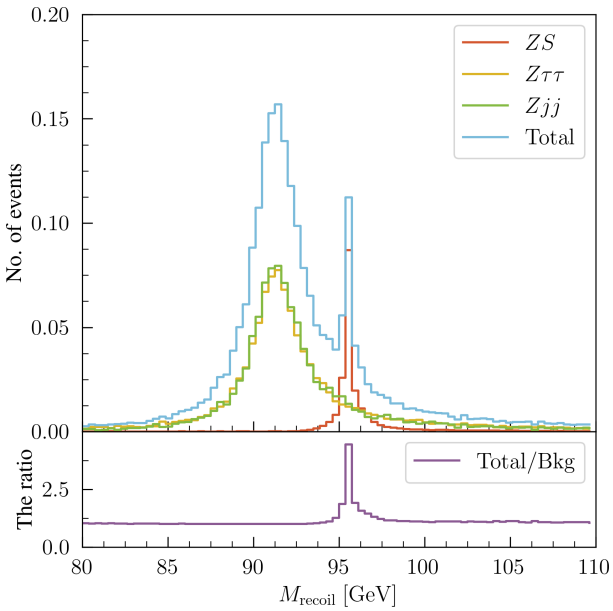

Fig. 1. (color online) Recoil mass distributions for the signal process ZS with $M_S = 95.5$ (normalized to 0.2), backgrounds $Z\tau\tau$ and Zjj (normalized to 1), and total (signal + background). The lower panel shows the ratio of the total to the background.

dominated across the mass range, as further reflected in the lower panel, where the ratio of the total to the backgrounds exhibits a localized peak near the signal mass.

We scan the center-of-mass energy $\sqrt{s}$ from 190 to 240 GeV in 2 GeV steps and vary the scalar mass M_S from 94 to 100 GeV in 0.5 GeV increments. For illustration, we consider the signal cross section to be 20% of the corresponding SM process with $m_h = M_S$, as computed using MadGraph5_aMC@NLO_v3.4.2 [77, 78].

Event selection requires two identified muons to reconstruct $M_{\rm recoil}$ and at least one τ-tagged jet to suppress the Zjj background. A second τ-tag is not required, as its efficiency is limited and would significantly reduce the signal acceptance despite better background rejection [81]. Basic kinematic requirements are imposed on the muons:

$$\begin{aligned} p_{\rm T}(\mu) > 10\ {\rm GeV}, \quad & p_T(\tau) > 20\ {\rm GeV}, \\ |\eta(\mu)| < 2.5, \quad & \Delta R(\mu_1,\mu_2) > 0.4, \end{aligned} \tag{3}$$

where $p_{\rm T}$ and η denote the transverse momentum and pseudorapidity, respectively, and $\Delta R = \sqrt{(\Delta\eta)^2 + (\Delta\phi)^2}$ measures the angular separation of the muon pair. In addition, the recoil mass is required to lie within $|M_{\rm recoil} - M_S| < 1.5$ GeV to suppress the backgrounds further.

The basic selection suppresses the reducible Zjj background by roughly four orders of magnitude. Requiring $|M_{\rm recoil} - M_S| < 1.5$ GeV removes approximately 90% of the remaining Zjj and $Z\tau\tau$ events while retaining approximately 80% of the signal.

Figure 2 shows the signal significance $\mathcal{Z}$ in the $(\sqrt{s}, M_S)$ plane, evaluated for an integrated luminosity of $L = 500\ {\rm fb}^{-1}$. The significance is computed using the Poisson expression [83]

$$\mathcal{Z} = \sqrt{2L[(\mathcal{S}+\mathcal{B})\ln(1+\mathcal{S}/\mathcal{B}) - \mathcal{S}]}, \tag{4}$$

where $\mathcal{S}$ and $\mathcal{B}$ denote the signal and background cross sections, respectively. Approximately one million signal and background events are generated for each parameter point. After applying the cut to $M_{\rm recoil}$, the dominant SM background originates from $Z\tau\tau$, with approximately 40,000 events surviving. The uncertainty regarding the expected number of background events is approximately 1%, which translates to a variation of approximately 0.4% in the estimated signal significance. At low statistics, this uncertainty is much smaller than the statistical uncertainty. Furthermore, we test a more conservative scenario by varying the expected number of background events by ±10%. The corresponding change in the signal significance is less than 4.5%. We observe a moderate increase in $\mathcal{Z}$ with M_S, reflecting the more rapid decline in SM backgrounds at higher scalar masses. The optimal center-of-mass energy is found to be $\sqrt{s} \simeq 210$ GeV. At the benchmark point ($M_S = 95.5$ GeV and $\sqrt{s} = 210$ GeV), we obtain $\mathcal{Z} \approx 5.1\sigma$. Reaching the same significance at the CEPC design energy of 240 GeV would require a luminosity of approximately 720 fb^{-1}, approximately 1.4 times that required at 210 GeV.

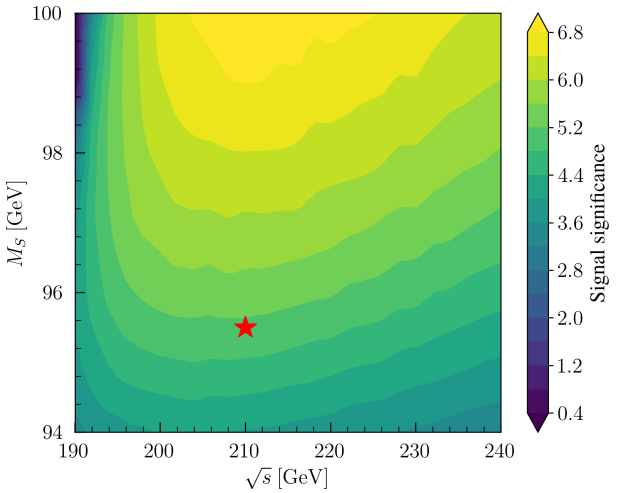

Fig. 2. (color online) Signal significance $\mathcal{Z}$ in the M_S versus $\sqrt{s}$ plane, assuming an integrated luminosity of 500 fb^{-1}. The red star indicates the benchmark point at $M_S = 95.5$ GeV and $\sqrt{s} = 210$ GeV.

III. MACHINE LEARNING TECHNIQUES

Despite the baseline cuts, the signal remains obscured by irreducible backgrounds, particularly from the $Z\tau\tau$ process. To enhance the sensitivity, we apply ML techniques at the benchmark points ($M_S = 95.5$ GeV, $\sqrt{s} = 210$ and 240 GeV), comparing three classifiers: XGBoost, GBDT, and DNN.

A set of 22 kinematic features is used as input, including:

- Four-momenta of μ_1, μ_2, and τ_1: E_{μ_1,μ_2,τ_1}, $p_x^{\mu_1,\mu_2,\tau_1}$, $p_y^{\mu_1,\mu_2,\tau_1}$, and $p_z^{\mu_1,\mu_2,\tau_1}$.

- Transverse momenta and pseudorapidities of μ_1, μ_2, and τ_1: $p_{\rm T}^{\mu_1,\mu_2,\tau_1}$ and $\eta_{\mu_1,\mu_2,\tau_1}$.

- Angular separations ΔR among μ_1, μ_2, and τ_1: $\Delta R[\mu_1,\mu_2]$, $\Delta R[\mu_1,\tau_1]$, and $\Delta R[\mu_2,\tau_1]$

- The recoil mass $M_{\rm recoil}$.

The DNN architecture consists of six hidden layers with 64, 48, 32, 24, 16, and 8 neurons, respectively. To mitigate overfitting and vanishing gradients, dropout with a rate of 20% is applied to the first two layers, and each hidden layer uses the Rectified Linear Unit (ReLU) activation function [84]. The output layer contains a single

neuron with sigmoid activation. Training is performed using the Adam optimizer with a learning rate of 0.0001. Approximately 200k events are used for training and evaluation, with 70% for training and 30% for testing. The training and testing are performed on an RTX 3060 GPU, and the DNN typically converges within minutes. The model reaches a test accuracy of approximately 77% after 10 epochs. Finally, it reaches a classification accuracy of 78% (77%) and an area under the ROC curve (AUC) of 0.87 (0.85) at $\sqrt{s} = 210\,(240)$ GeV. Inreasing the size of the training set further mainly improves the stability of the training process while offering limited gains in classification accuracy. Significant additional improvements would likely require more advanced ML architectures or direct access to particle-level information, which we leave for future work.

Figure 3 shows the integrated luminosity required to achieve a 5σ significance at the benchmark point as a function of the signal efficiency before and after applying the ML classifiers. Here, the signal efficiency is defined as the true positive rate (TPR):

$$\mathrm{TPR} = \frac{N_{\mathrm{TP}}}{N_{\mathrm{TP}} + N_{\mathrm{FN}}}, \tag{5}$$

where N_{TP} is the number of correctly classified signal events, and N_{FN} is the number of signal events that are misclassified as background. This quantity characterizes the efficiency of the ML classifier in recognizing signal events. The green, red, yellow, and blue curves (dotted for $\sqrt{s} = 240$ GeV) correspond to the baseline selection

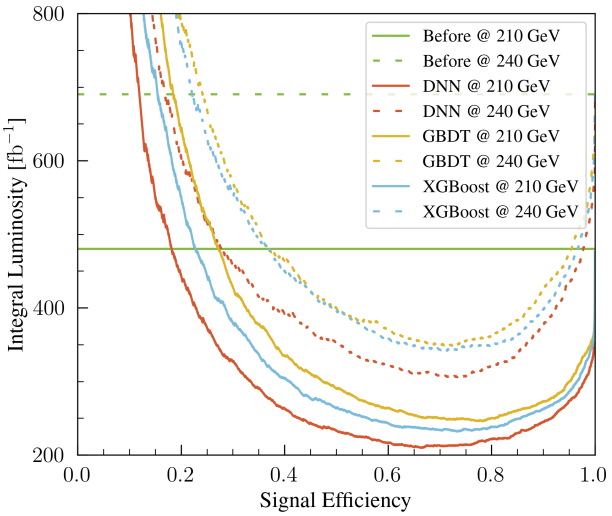

Fig. 3. (color online) Integrated luminosity required to reach 5σ significance at the benchmark point as a function of the signal efficiency. The solid (dotted) curves correspond to $\sqrt{s} = 210\,(240)$ GeV. The colors denote different selection strategies: baseline (before applying ML classifiers; green), DNN (red), GBDT (yellow), and XGBoost (blue).

(before applying the ML classifiers), DNN, GBDT, and XGBoost, respectively, at $\sqrt{s} = 210$ GeV. At each energy, the DNN consistently requires the lowest luminosity for any given signal efficiency. The minimum required luminosity is attained at a signal efficiency of approximately 0.66 (0.74) for $\sqrt{s} = 210\,(240)$ GeV with the DNN, reducing the required luminosity from 480 (690) fb^{-1} in the baseline to less than 210 (310) fb^{-1}. The full cut flow with $L = 500$ fb^{-1} is summarized in Table 1.

Figure 4 shows the CEPC coverage (left panel) and detection precision (right panel) in the $\mathrm{Br}(S \to \tau^+\tau^-)$ versus C_{SZZ} planes for $\sqrt{s} = 210$ GeV (solid line) and 240 GeV (dashed line), with an integrated luminosity of $L = 20$ ab^{-1}. Here, C_{SZZ} denotes the reduced coupling of SZZ in the N2HDM-Flipped to its SM value. The left panel presents the expected 2σ and 5σ significance contours. The right panel displays the relative statistical precision on the signal yield, evaluated as

$$\delta_{\mathrm{stat}} = \frac{\sqrt{(\mathcal{S}+\mathcal{B})L}}{\mathcal{S}L}, \tag{6}$$

where $\mathcal{S}$ and $\mathcal{B}$ denote the signal and background cross sections, respectively. The primary sources of systematic uncertainty include τ-jet reconstruction, jet energy scale and resolution, and theoretical uncertainties in the cross-section and shape predictions. Based on the CEPC Technical Design Report and related studies [39, 85, 86], we estimate the overall systematic uncertainty to be approximately 2%. Therefore, the statistical uncertainty dominates until it decreases below this level. As the production rate in the Higgs-strahlung channel $e^+e^- \to ZS(\to \tau^+\tau^-)$ is controlled by both the ZS coupling and branching fraction of $S \to \tau^+\tau^-$, it is convenient to introduce the signal strength

$$\mu_{\tau\tau}^{ZS} \equiv C_{SZZ}^2 \cdot \frac{\mathrm{Br}(S \to \tau^+\tau^-)}{\mathrm{Br}_{\mathrm{SM}}(h_{95} \to \tau^+\tau^-)}. \tag{7}$$

This single parameter encapsulates the combined dependence on C_{SZZ} and $\mathrm{Br}(S \to \tau^+\tau^-)$ and is used to present the CEPC sensitivity. In this parameterization,

Table 1. Cut flow of signal and background events (in units of events per 500 fb^{-1}) for $\sqrt{s} = 210\,(240)$ GeV. The numbers in parentheses refer to the 240 GeV case. The final column lists the resulting signal significance $\mathcal{Z}$.

Cuts	ZS	$Z\tau\tau$	Zjj	$\mathcal{Z}[\sigma]$
Initial	134 (109)	1819 (1769)	24187 (21745)	0.83 (0.71)
Basic	59.7 (52.7)	780.2 (816.7)	49.4 (4.7)	2.0 (1.8)
M_{recoil}	47.4 (38.7)	66.0 (66.0)	5.2 (4.7)	5.1 (4.3)
ML	31.5 (28.6)	8.2 (11.5)	0.6 (0.8)	7.7 (6.4)

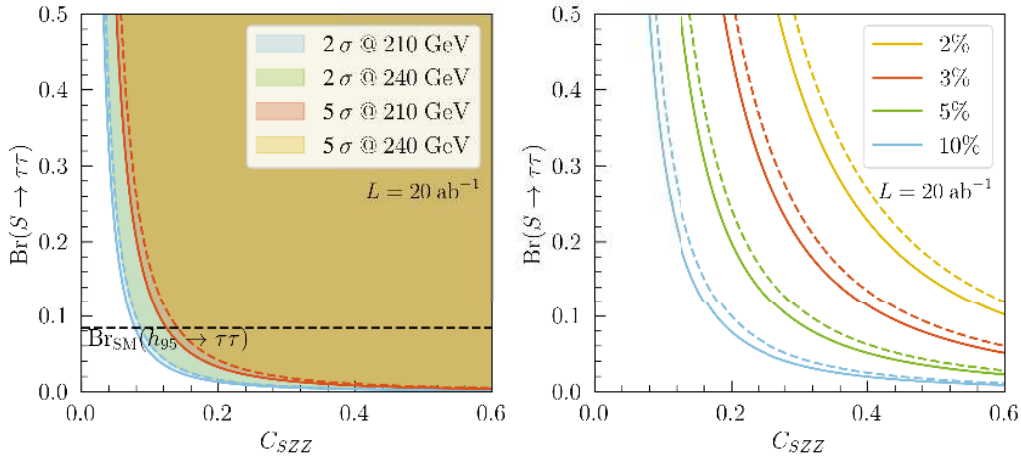

Fig. 4. (color online) CEPC sensitivity in the $\mathrm{Br}(S \to \tau^+\tau^-)$ versus C_{SZZ} planes. The left panel shows the expected 2σ and 5σ coverage, and the right panel shows the relative statistical precision of the signal yield. Results are presented for $\sqrt{s} = 210$ GeV (solid) and $\sqrt{s} = 240$ GeV (dashed), assuming an integrated luminosity of $L = 20\ \mathrm{ab}^{-1}$.

CEPC can investigate $\mu_{\tau\tau}^{ZS} > 0.016$ (0.020) at 5σ and > 0.006 (0.008) at 2σ for $\sqrt{s} = 210$ (240) GeV. The right panel shows that percent-level precision of $\mu_{\tau\tau}^{ZS}$ can be achieved once this quantity reaches $O(10^{-2})$. The corresponding values of $\mu_{\tau\tau}^{ZS}$ that are required to obtain the selected precision targets are summarized in Table 2. Furthermore, Ref. [37] indicates that the HL-LHC, with an integrated luminosity of 3 ab^{-1}, can reach a 5σ discovery for the process $pp \to t\bar{t}S(\to \gamma\gamma)$, provided that the cross section exceeds approximately 0.3 fb. In addition, a 5 ab^{-1} CEPC run is projected to be able to cover the current $\sim 2\sigma$ excess at the 5σ level through the channel $e^+e^- \to Z(\mu^+\mu^-)S(\to b\bar{b})$ [39]. Together with our present study, these projections outline a promising and complementary path toward probing the potential BSM origin of the 95 GeV resonance at future colliders.

Table 2. Signal strength $\mu_{\tau\tau}^{ZS}$ required to reach the indicated relative statistical precision of the signal yield at $\sqrt{s} = 210$ and 240 GeV with $L = 20\ \mathrm{ab}^{-1}$.

Target Precision	Required $\mu_{\tau\tau}^{ZS}$ (210 GeV)	Required $\mu_{\tau\tau}^{ZS}$ (240 GeV)
10%	0.04	0.05
5%	0.10	0.12
3%	0.22	0.26
2%	0.44	0.52

IV. N2HDM-FLIPPED

To demonstrate the broader applicability of our ML approach, we examine the sensitivity of the CEPC to the parameter space of the N2HDM-Flipped. The same strategy can also be straightforwardly applied to other models with an extended Higgs sector, such as the next-to-minimal supersymmetric model (NMSSM). The N2HDM-Flipped extends the SM with a second Higgs doublet and a real singlet, where the Yukawa coupling of charged leptons is "flipped" from down- (in the Type-II N2HDM or NMSSM) to up-quark-like [87–89]. A complete definition of the N2HDM-Flipped is provided in Section II of Ref. [24], which details its particle content, coupling structure, and differences from scenarios of other types. Ref. [32] shows that the N2HDM-Flipped scenario can accommodate the excesses observed in several channels. The present study further evaluates the CEPC detection potential for the surviving parameter space of this model.

Following electroweak symmetry breaking, three neutral CP-even states $H_{a,b,c}$, a pseudoscalar A, and a charged pair $H^\pm$ exist in the N2HDM-Flipped. We identify H_a using the 125 GeV SM like Higgs boson and consider H_b as the putative 95 GeV resonance. In total, 11 new parameters need to be defined: the masses of $H_{a,b,c}$, A, and $H^\pm$; the ratio of the vacuum expected values (VEV) of two Higgs doublets $\tan\beta$; the effective couplings of H_a to massive gauge bosons ($C^2_{H_aVV}$) and top-quarks ($C^2_{H_att}$); the mixing matrix elements between $H_{a,b}$ and the singlet field (R^{in}_{a3} and R^{in}_{b3}); the soft Z_2-breaking parameter m^2_{12}; and the singlet VEV v_S. The 11 independent parameters are scanned in the following ranges:

$$
\begin{aligned}
&95 < m_{H_b} < 96\ \mathrm{GeV}, && \mathrm{sign}(R^{\mathrm{in}}_{a3}) = \pm 1,\\
&300 < m_{H_c,A} < 1500\ \mathrm{GeV}, && 580 < m_{H^\pm} < 1500\ \mathrm{GeV},\\
&0.8 < \tan\beta < 10, && -1 < R^{\mathrm{in}}_{b3} < 1,\\
&0.70 < C^2_{H_aVV} < 1.00, && 0.70 < C^2_{H_att} < 1.20,\\
&10^{-3} < m^2_{12} < 5\times 10^5\ \mathrm{GeV}^2, && 1 < v_S < 3000\ \mathrm{GeV}.
\end{aligned}
\tag{8}
$$

For each parameter point, we impose theoretical con-

sistency conditions, including perturbative unitarity, vacuum stability, and perturbativity, as well as current experimental constraints from Higgs, flavor, and electroweak precision observables. The parameter scan is performed using ScannerS_v2.0.0 [90, 91], which interfaces with HiggsBounds_v5.10.0 [92, 93], HiggsSignals_v2.6.0 [94, 95], and SuperIso_v4.1 [96, 97] to evaluate physical observables and apply the relevant constraints [89, 98–104]. This study uses a profiled likelihood ratio test with the SM as the alternative hypothesis, defining $\Delta\chi^2 = \chi^2_{\rm N2HDM} - \chi^2_{\rm SM}$ and requiring $\Delta\chi^2 < 6.18$ at a 95% confidence level, where $\chi^2_{\rm N2HDM}$ and $\chi^2_{\rm SM}$ are provided by HiggsSignals, to evaluate the compatibility of the 125 GeV Higgs with the experimental data [95].

We further perform a $\chi^2_{h_{95}}$ analysis to evaluate the compatibility of the N2HDM-Flipped with the observed excesses in the $\tau^+\tau^-$, $b\bar{b}$, and $\gamma\gamma$ channels. This is not a discovery test but rather a goodness-of-fit check to determine whether the model is compatible with the existing experimental hints. $\chi^2_{h_{95}}$ is defined as

$$\chi^2_{h_{95}} = \sum_{xx=\tau\tau,\gamma\gamma,bb} \frac{(\mu_{xx} - \mu^{\rm exp}_{xx})^2}{(\Delta\mu^{\rm exp}_{xx})^2}, \tag{9}$$

where μ_{xx} denotes the model prediction, and $\mu^{\rm exp}_{xx} \pm \Delta\mu^{\rm exp}_{xx}$ are the experimentally measured signal strengths and uncertainties, respectively, as specified in Eq. (1). The uncertainties of the three excesses are treated at the 1σ level, and the requirement $\chi^2_{h_{95}} < 7.82$ corresponds to consistency with the experimental results at the 95% confidence level for three degrees of freedom, indicating that the model is not excluded by current data within this statistical tolerance.

After applying the abovementioned constraints, surviving samples with $\chi^2_{h_{95}} < 7.82$ in the $\mu_{\tau\tau}$ versus $\mu_{\gamma\gamma}$ plane for $\sqrt{s} = 210$ (left) and 240 (right) GeV are shown in Fig. 5. The CEPC with $L = 100$, 200, 800 fb^{-1}, and 1.22 ab^{-1} can cover the red, yellow, blue, and green samples at the 5σ level, respectively. All surviving samples can be covered at 5σ for $\sqrt{s} = 210$ GeV with $L = 800$ fb^{-1} and $\sqrt{s} = 240$ GeV with $L = 1.22$ ab^{-1}. The green and purple regions in Fig. 5 indicate the 1σ excesses in the $\tau^+\tau^-$ and $\gamma\gamma$ channels, respectively, as reported by experiments. The best-fit point, marked by a red star, yields $\chi^2_{h_{95}} = 0.24$, corresponding to a p-value of 0.971. For this point, a 2σ sensitivity can be achieved with $L = 10$ fb^{-1} and 5σ with $L = 58$ fb^{-1} at $\sqrt{s} = 210$ GeV. At $\sqrt{s} = 240$ GeV, the same levels of sensitivity require $L = 13$ fb^{-1} and $L = 80$ fb^{-1}, respectively. Apart from the sensitivity projections in Fig. 5 and the associated discussion, our analysis is independent of the specific selection of $\mu_{\tau\tau}$. A smaller consistent $\mu_{\tau\tau}$ would require a correspondingly higher integrated luminosity to maintain equivalent coverage of the parameter space that is compatible with the current excesses. These results demonstrate that the $e^+e^- \to Z(\to \mu^+\mu^-)S(\to \tau^+\tau^-)$ channel at the CEPC offers excellent potential to probe the 95 GeV excess in the N2HDM-Flipped framework.

V. CONCLUSIONS AND OUTLOOK

Our study has identified $\sqrt{s} = 210$ GeV as the optimal center-of-mass energy to investigate a hypothetical scalar with a mass of 95 GeV or slightly higher. Without ML techniques, the benchmark point requires integrated luminosities of 480(690) fb^{-1} to reach a 5σ significance at $\sqrt{s} = 210(240)$ GeV. A DNN classifier can reduce

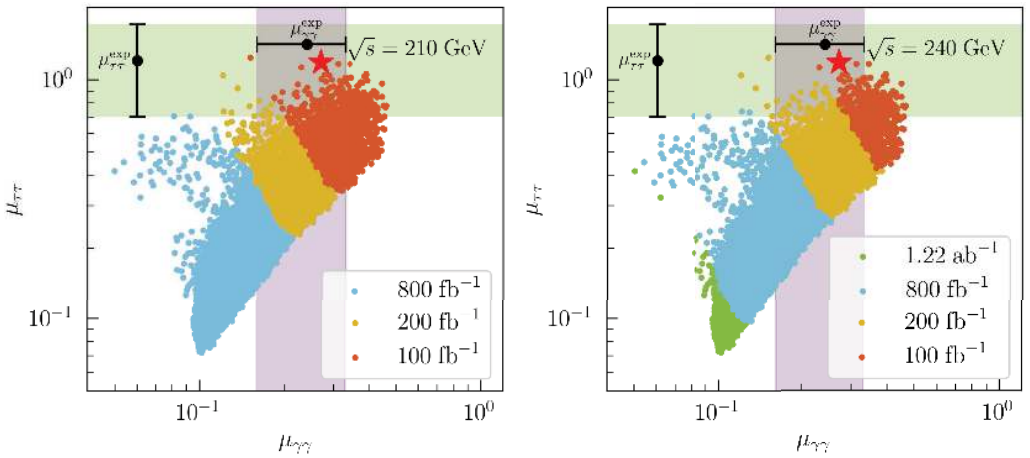

Fig. 5. (color online) Coverage ability of the CEPC for surviving samples in the $\mu_{\tau\tau}$ versus $\mu_{\gamma\gamma}$ plane at $\sqrt{s} = 210$ GeV (left panel) and $\sqrt{s} = 240$ GeV (right panel). The CEPC with $L = 100$, 200, 800 fb^{-1}, and 1.22 ab^{-1} can cover the red, yellow, blue, and green samples at the 5σ level, respectively. All surviving samples can be covered at 5σ for $\sqrt{s} = 210$ GeV with $L = 800$ fb^{-1} and $\sqrt{s} = 240$ GeV with $L = 1.22$ ab^{-1}. The red star marks the best-fit point. The green and purple shaded bands indicate the experimental 1σ ranges for the $\tau^+\tau^-$ and $\gamma\gamma$ channels, respectively.

these values to 210(310) fb^{-1} at the corresponding energies. At $L = 20$ ab^{-1}, the 5σ sensitivity of the CEPC to the signal strength $\mu_{\tau\tau}^{ZS}$ reaches 0.016 and 0.020 for $\sqrt{s} = 210$ GeV and 240 GeV, respectively. The corresponding thresholds for a 5% precision measurement are $\mu_{\tau\tau}^{ZS} > 0.10$ and > 0.12. At $\sqrt{s} = 210$ GeV (240 GeV), 5σ coverage of all N2HDM-Flipped samples with $\chi^2_{h_{95}} < 7.82$ requires $L = 800$ fb^{-1} (1.22 ab^{-1}). These results suggest that an early CEPC run at 210 GeV, combined with modern ML selection, offers the most efficient strategy for probing the 95 GeV excess. The analysis framework can be readily adapted to alternative lepton colliders such as the ILC and FCC-ee and adjusted to other light-scalar scenarios.

References

[1] S. Chatrchyan *et al.* (CMS Collaboration), Phys. Lett. B **716**, 30 (2012), arXiv: 1207.7235[hep-ex]
[2] G. Aad *et al.* (ATLAS Collaboration), Phys. Lett. B **716**, 1 (2012), arXiv: 1207.7214[hep-ex]
[3] A. D. Sakharov, Pisma Zh. Eksp. Teor. Fiz. **5**, 32 (1967)
[4] X.-m. Zhang, Phys. Rev. D **47**, 3065 (1993), arXiv: hepph/9301277
[5] K. Kajantie, M. Laine, K. Rummukainen *et al.*, Nucl. Phys. B **466**, 189 (1996), arXiv: hep-lat/9510020
[6] R. Barate *et al.* (LEP Working Group for Higgs boson searches, ALEPH, DELPHI, L3, OPAL Collaborations), Phys. Lett. B **565**, 61 (2003), arXiv: hep-ex/0306033
[7] A. Hayrapetyan *et al.* (CMS Collaboration), Phys. Lett. B **860**, 139067 (2025), arXiv: 2405.18149[hep-ex]
[8] G. Aad *et al.* (ATLAS Collaboration), JHEP **01**, 053 (2025), arXiv: 2407.07546[hep-ex]
[9] A. Tumasyan *et al.* (CMS Collaboration), JHEP **07**, 073 (2023), arXiv: 2208.02717[hep-ex]
[10] T. Biekötter, S. Heinemeyer, and G. Weiglein, Phys. Rev. D **109**, 035005 (2024), arXiv: 2306.03889[hep-ph]
[11] CMS Collaboration, CMS-PAS-EXO-21-018 (2022).
[12] A. Kundu, S. Maharana, and P. Mondal, Nucl. Phys. B **955**, 115057 (2020), arXiv: 1907.12808[hep-ph]
[13] Z.-f. Ge, F.-Y. Niu, and J.-L. Yang, Eur. Phys. J. C **84**, 548 (2024), arXiv: 2405.07243[hep-ph]
[14] J. A. Aguilar-Saavedra and F. R. Joaquim, Eur. Phys. J. C **80**, 403 (2020), arXiv: 2002.07697[hep-ph]
[15] S. Yaser Ayazi, M. Hosseini, S. Paktinat Mehdiabadi *et al.*, Phys. Rev. D **110**, 055004 (2024), arXiv: 2405.01132[hep-ph]
[16] L. Liu, H. Qiao, K. Wang *et al.*, Chin. Phys. C **43**, 023104 (2019), arXiv: 1812.00107[hep-ph]
[17] K. Wang and J. Zhu, Chin. Phys. C **48**, 073105 (2024), arXiv: 2402.11232[hep-ph]
[18] P. Escribano, V. M. Lozano, and A. Vicente, Phys. Rev. D **108**, 115001 (2023), arXiv: 2306.03735[hep-ph]
[19] D. Borah, S. Mahapatra, P. K. Paul *et al.*, Phys. Rev. D **109**, 055021 (2024), arXiv: 2310.11953[hep-ph]
[20] P. S. B. Dev, R. N. Mohapatra, and Y. Zhang, Phys. Lett. B **849**, 138481 (2024), arXiv: 2312.17733[hep-ph]
[21] A. Ahriche, M. L. Bellilet, M. O. Khojali *et al.*, Phys. Rev. D **110**, 015025 (2024), arXiv: 2311.08297[hep-ph]
[22] A. A. Abdelalim, B. Das, S. Khalil *et al.*, Nucl. Phys. B **985**, 116013 (2022), arXiv: 2012.04952[hep-ph]
[23] S. Ashanujjaman, S. Banik, G. Coloretti *et al.*, Phys. Rev. D **108**, L091704 (2023), arXiv: 2306.15722[hep-ph]
[24] T. Biekötter, M. Chakraborti, and S. Heinemeyer, Eur. Phys. J. C **80**, 2 (2020), arXiv: 1903.11661[hep-ph]
[25] A. Khanna, S. Moretti, and A. Sarkar,Nucl. Phys. B **1022**, 117229 (2026), arXiv: 2409.02587[hep-ph]
[26] R. Benbrik, M. Boukidi, K. Kahime *et al.*, Phys. Lett. B **868**, 139688 (2025), arXiv: 2505.07811[hep-ph]
[27] T. Biekötter, A. Grohsjean, S. Heinemeyer *et al.*, Eur. Phys. J. C **82**, 178 (2022), arXiv: 2109.01128[hep-ph]
[28] S. Banik, A. Crivellin, S. Iguro *et al.*, Phys. Rev. D **108**, 075011 (2023), arXiv: 2303.11351[hep-ph]
[29] J. A. Aguilar-Saavedra, H. B. Câmara, F. R. Joaquim *et al.*, Phys. Rev. D **108**, 075020 (2023), arXiv: 2307.03768[hep-ph]
[30] S. Heinemeyer, C. Li, F. Lika *et al.*, Phys. Rev. D **106**, 075003 (2022), arXiv: 2112.11958[hep-ph]
[31] T. Biekötter and M. O. Olea-Romacho, JHEP **10**, 215 (2021), arXiv: 2108.10864[hep-ph]
[32] T. Biekötter, S. Heinemeyer, and G. Weiglein, JHEP **08**, 201 (2022), arXiv: 2203.13180[hep-ph]
[33] T. Biekötter, S. Heinemeyer, and G. Weiglein, Eur. Phys. J. C **83**, 450 (2023), arXiv: 2204.05975[hep-ph]
[34] T. Biekötter, S. Heinemeyer, and G. Weiglein, Phys. Lett. B **846**, 138217 (2023), arXiv: 2303.12018[hep-ph]
[35] G. Arcadi, G. Busoni, D. Cabo-Almeida *et al.*, Phys. Rev. D **110**, 115028 (2024), arXiv: 2311.14486[hep-ph]
[36] A. M. Coutinho, A. Karan, V. Miralles *et al.*, JHEP **02**, 057 (2025), arXiv: 2412.14906[hep-ph]
[37] Y. Dong, K. Wang, and J. Zhu, Phys. Rev. D **112**, 055013 (2025), arXiv: 2410.13636[hep-ph]
[38] S. Banik, G. Coloretti, A. Crivellin *et al.*, Phys. Rev. D **111**, 075021 (2025), arXiv: 2412.00523[hep-ph]
[39] P. Sharma, A.-T. Mulaudzi, K. Mosala *et al.*,Phys. Lett. **870**, 139953 (2025), arXiv: 2407.16806 [hep-ph]
[40] J. Dutta, J. Lahiri, C. Li *et al.*, (2025), arXiv: 2504.14529[hep-ph]
[41] H. Xu, Y. Wang, X.-F. Han *et al.*,Chin. Phys. C **50**, 013108 (2026), arXiv: 2505.03592[hep-ph]
[42] R. Benbrik, M. Boukidi, and S. Moretti, Phys. Rev. D **110**, 115030 (2024), arXiv: 2405.02899[hep-ph]
[43] R. Benbrik, M. Boukidi, S. Moretti *et al.*, Phys. Lett. B **832**, 137245 (2022), arXiv: 2204.07470[hep-ph]
[44] T. Biekötter, M. Chakraborti, and S. Heinemeyer, Int. J. Mod. Phys. A **36**, 2142018 (2021), arXiv: 2003.05422 [hep-ph]
[45] S. Iguro, T. Kitahara, Y. Omura *et al.*, Phys. Rev. D **107**, 075017 (2023), arXiv: 2211.00011[hep-ph]
[46] D. Azevedo, T. Biekötter, and P. M. Ferreira, JHEP **11**, 017 (2023), arXiv: 2305.19716[hep-ph]
[47] A. Belyaev, R. Benbrik, M. Boukidi *et al.*, JHEP **05**, 209 (2024), arXiv: 2306.09029[hep-ph]
[48] G. Coloretti, A. Crivellin, and B. Mellado, Phys. Rev. D **110**, 073001 (2024), arXiv: 2312.17314[hep-ph]
[49] M. Maniatis and O. Nachtmann, Phys. Rev. D **111**, 055009 (2025), arXiv: 2309.04869[hep-ph]
[50] J. Cao, X. Guo, Y. He *et al.*, Phys. Rev. D **95**, 116001 (2017), arXiv: 1612.08522[hep-ph]
[51] K. Wang, F. Wang, J. Zhu *et al.*, Chin. Phys. C **42**, 103109 (2018), arXiv: 1811.04435[hep-ph]

[52] J. Cao, X. Jia, Y. Yue *et al.*, Phys. Rev. D **101**, 055008 (2020), arXiv: 1908.07206[hep-ph]
[53] W. G. Hollik, C. Li, G. Moortgat-Pick *et al.*, Eur. Phys. J. C **81**, 141 (2021), arXiv: 2004.14852[hepph]
[54] W. Li, H. Qiao, and J. Zhu, Chin. Phys. C **47**, 123102 (2023), arXiv: 2212.11739[hep-ph]
[55] F. Domingo, U. Ellwanger, and C. Hugonie, Eur. Phys. J. C **82**, 1074 (2022), arXiv: 2209.03863[hep-ph]
[56] J. Cao, X. Jia, J. Lian *et al.*, Phys. Rev. D **109**, 075001 (2024), arXiv: 2310.08436[hep-ph]
[57] W. Li, H. Qiao, K. Wang *et al.*, (2023), arXiv: 2312.17599[hep-ph]
[58] J. Lian, Phys. Rev. D **110**, 115018 (2024), arXiv: 2406.10969[hep-ph]
[59] J. Cao, X. Jia, and J. Lian, Phys. Rev. D **110**, 115039 (2024), arXiv: 2402.15847[hep-ph]
[60] U. Ellwanger and C. Hugonie, Eur. Phys. J. C **83**, 1138 (2023), arXiv: 2309.07838[hep-ph]
[61] U. Ellwanger, C. Hugonie, S. F. King *et al.*, Eur. Phys. J. C **84**, 788 (2024), arXiv: 2404.19338[hepph]
[62] K. Choi, S. H. Im, K. S. Jeong *et al.*, Eur. Phys. J. C **79**, 956 (2019), arXiv: 1906.03389[hep-ph]
[63] U. Ellwanger and C. Hugonie, Eur. Phys. J. C **84**, 526 (2024), arXiv: 2403.16884[hep-ph]
[64] C. Wang, J. Q. Tao, M. A. Shahzad *et al.*, Chin. Phys. C **46**, 083107 (2022), arXiv: 2204.09198[hep-ph]
[65] T. K. Chen, C. W. Chiang, S. Heinemeyer *et al.*, Phys. Rev. D **109**, 075043 (2024), arXiv: 2312.13239[hep-ph]
[66] A. Ahriche, Phys. Rev. D **110**, 035010 (2024), arXiv: 2312.10484[hep-ph]
[67] R. Ghosh and B. Mukhopadhyaya, Phys. Rev. D **107**, 035031 (2023), arXiv: 2212.11688[hep-ph]
[68] P. Mondal and S. Samanta, (2025), arXiv: 2506.06427 [hep-ph]
[69] P. Drechsel, G. Moortgat-Pick, and G. Weiglein, Eur. Phys. J. C **80**, 922 (2020), arXiv: 1801.09662[hep-ph]
[70] Y. Wang, J. List, and M. Berggren (2018), arXiv: 1801.08164[hep-ex]
[71] B. Brudnowski, K. Zembaczyński, and A. F. Żarnecki, EPJ Web Conf. **315**, 01026 (2024), arXiv: 2409.19761[hep-ph]
[72] G. C. Branco, P. M. Ferreira, L. Lavoura *et al.*, Phys. Rept. **516**, 1 (2012), arXiv: 1106.0034[hep-ph]
[73] M. Dong *et al.* (CEPC Study Group), (2018), arXiv: 1811.10545[hep-ex]
[74] CEPC Study Group, (2018), arXiv: 1809.00285 [physics.acc-ph]
[75] F. F. An, Y. Bai, C. H. Chen *et al.*, Chin. Phys. C **43**, 043002 (2019), arXiv: 1810.09037[hep-ex]
[76] W. Abdallah *et al.* (CEPC Study Group),Radiat. Detect. Technol. Methods **8**, 1 (2024), [Erratum: Radiat. Detect. Technol. Methods 9, 184-192(2025)], arXiv: 2312.14363[physics.acc-ph]
[77] J. Alwall, M. Herquet, F. Maltoni *et al.*, JHEP **06**, 128 (2011), arXiv: 1106.0522[hepph]
[78] J. Alwall, R. Frederix, S. Frixione *et al.*, JHEP **07**, 079 (2014), arXiv: 1405.0301[hep-ph]
[79] T. Sjöstrand, S. Ask, J. R. Christiansen *et al.*, Comput. Phys. Commun. **191**, 159 (2015), arXiv: 1410.3012[hep-ph]
[80] J. de Favereau *et al.* (DELPHES 3 Collaboration), JHEP **02**, 057 (2014), arXiv: 1307.6346[hep-ex]
[81] D. Yu, M. Ruan, V. Boudry *et al.*, Eur. Phys. J. C **80**, 7 (2020)
[82] Z. Chen, Y. Yang, M. Ruan *et al.*, Chin. Phys. C **41**, 023003 (2017), arXiv: 1601.05352[hep-ex]
[83] G. Cowan, K. Cranmer, E. Gross *et al.*, Eur. Phys. J. C **71**, 1554 (2011), arXiv: 1007.1727[physics.data-an]
[84] A. F. Agarap, (2018), arXiv: 1803.08375[cs.NE]
[85] S. P. Adhya *et al.* (CEPC Study Group), (2025), arXiv: 2510.05260[hep-ex]
[86] X. Ma, Z. Wu, J. Wu *et al.*, Chin. Phys. C **49**, 053001 (2025), arXiv: 2410.04465[hep-ex]
[87] C.-Y. Chen, M. Freid, and M. Sher, Phys. Rev. D **89**, 075009 (2014), arXiv: 1312.3949[hep-ph]
[88] A. Drozd, B. Grzadkowski, J. F. Gunion *et al.*, JHEP **11**, 105 (2014), arXiv: 1408.2106[hep-ph]
[89] M. Muhlleitner, M. O. P. Sampaio, R. Santos *et al.*, JHEP **03**, 094 (2017), arXiv: 1612.01309[hep-ph]
[90] R. Coimbra, M. O. P. Sampaio, and R. Santos, Eur. Phys. J. C **73**, 2428 (2013), arXiv: 1301.2599[hep-ph]
[91] M. Mühlleitner, M. O. P. Sampaio, R. Santos *et al.*, Eur. Phys. J. C **82**, 198 (2022), arXiv: 2007.02985[hep-ph]
[92] P. Bechtle, O. Brein, S. Heinemeyer *et al.*, Comput. Phys. Commun. **181**, 138 (2010), arXiv: 0811.4169[hep-ph]
[93] P. Bechtle, D. Dercks, S. Heinemeyer *et al.*, Eur. Phys. J. C **80**, 1211 (2020), arXiv: 2006.06007[hep-ph]
[94] P. Bechtle, S. Heinemeyer, O. Stål *et al.*, Eur. Phys. J. C **74**, 2711 (2014), arXiv: 1305.1933[hep-ph]
[95] P. Bechtle, S. Heinemeyer, T. Klingl *et al.*, Eur. Phys. J. C **81**, 145 (2021), arXiv: 2012.09197[hep-ph]
[96] F. Mahmoudi, Comput. Phys. Commun. **178**, 745 (2008), arXiv: 0710.2067[hep-ph]
[97] F. Mahmoudi, Comput. Phys. Commun. **180**, 1579 (2009), arXiv: 0808.3144[hep-ph]
[98] M. E. Peskin and T. Takeuchi, Phys. Rev. Lett. **65**, 964 (1990)
[99] M. E. Peskin and T. Takeuchi, Phys. Rev. D **46**, 381 (1992)
[100] S. Kanemura, T. Kubota, and E. Takasugi, Phys. Lett. B **313**, 155 (1993), arXiv: hep-ph/9303263
[101] A. G. Akeroyd, A. Arhrib, and E.-M. Naimi, Phys. Lett. B **490**, 119 (2000), arXiv: hep-ph/0006035
[102] A. Arhrib, (2000), arXiv: hep-ph/0012353
[103] A. W. El Kaffas, W. Khater, O. M. Ogreid *et al.*, Nucl. Phys. B **775**, 45 (2007), arXiv: hepph/0605142
[104] R. L. Workman *et al.* (Particle Data Group), PTEP **2022**, 083C01 (2022)